# A Consolidated Theory for Predicting Rain Noise

*by*

**Daniel Griffin, Keith Ballagh**

# A Consolidated Theory for Predicting Rain Noise

**Daniel Griffin, Keith Ballagh**

*Marshall Day Acoustics, PO Box 5811 Wellesley Street, Auckland 1141, New Zealand*
*dgriffin@marshallday.com, keith.ballagh@marshallday.co.nz*

**ABSTRACT**

This paper presents a theory for rain noise prediction, consolidating discussions of drop impact on a plate and resulting work on rain noise predictions that is found in the literature. An objective of the consolidated theory is a robust engineering model which does not rely on complex computational techniques or lengthy computer simulation. The model described is compared to measured data to establish accuracy and reliability.

## 1.0 INTRODUCTION

The increasing prominence of rain noise as an assessable acoustic issue is evidenced by the publication of *International Standard 140-18:2006 Acoustics - Measurement of sound insulation in buildings and of building elements - Part 18: Laboratory measurement of sound generated by rainfall on building elements* (ISO 140-18) [1] in 2006 as well as the discussion of rain noise in various guidance documents such as *Building Bulletin 93 Acoustic design of schools* which was published in the United Kingdom in 2004, *Acoustic performance standards for the priority schools building programme* which was published in the United Kingdom in 2012 and the BREEAM Education 2008 assessor manual.

This paper presents a review of theory for rain noise prediction, consolidating discussions of drop impact on a plate and resulting work on rain noise predictions that is found in various research papers and texts [2], [3], [4], [5] to present an engineering model for rain noise prediction which does not rely on complex computational techniques or lengthy computer simulation. Section 2.0 begins with a brief over view of the theory in order to introduce key factors in the model such as the force, and impedance. Subsequent subsections provide a more detailed discussion of each of the identified factors. The discussion of force includes considerations in both the time and frequency domains. Discussion for the other key items is based in the frequency domain unless otherwise noted. The resulting rain noise prediction model is compared to a limited set of measured data in Section 3.0 to assess its accuracy and reliability.

## 2.0 THEORY
### 2.1 Overview
*Assumptions and limitations*
The focus of this paper is the prediction of rain noise levels in the building acoustics frequency range, typically 100-5000Hz, although with some consideration the model could be extended to encompass both lower and higher frequencies.

The reaction of a plate to a point force is considered initially. The resulting model is applied to the impact force of a single water drop on the plate. For comparison with measured data, the model is extended to consider rainfall on a roof, as the linear sum of individual drops. The predicted level of rain noise is determined as a function of the vibration velocity of the plate induced by rainfall. The vibration velocity is presented as the sum of:

- The resonant vibration velocity.
  Also referred to as the spatial-average or area-averaged velocity, which quantifies the free or resonant vibrations of a finite plate, generated from reflections of the wave field at the plate boundaries. The resonant vibration velocity is analogous to a reverberant sound pressure field in a room.

- The non-resonant vibration velocity.
  This quantifies the direct bending wave vibrations, also referred to as forced or bending wave near field vibrations, of the plate which will be considered herein below the critical frequency. The non-resonant vibration velocity is analogous to the direct, radiated sound pressure field from a source in air.

Unless otherwise noted, the plates discussed are assumed to be thin, isotropic and homogeneous.

*Model outline*
A discussion of the vibration response of a plate excited by a point force can be found in most reference texts ([6], [7], [8], [2]). The driving-point impedance $Z_{dp}$ of the plate, by definition, describes the relationship between a point force, acting perpendicular to the plate, and the resulting velocity of the plate at the driving point:

$$Z_{dp} = \frac{1}{Y_{dp}} = \frac{F_p}{v_{dp}} \tag{1}$$

Where $F_p$ is the point force (N), $v_{dp}$ is the resultant velocity (m/s) of the plate at the driving point and Y is the reciprocal of the impedance, termed mobility or admittance. Re-arranging eqn (1) provides an expression for the velocity of the plate at the driving point:

$$v_{dp} = F_p \cdot Y_{dp} = \frac{F_p}{Z_{dp}} \qquad (2)$$

$v_{dp}$ can be evaluated provided that $F_p$ and $Y_{dp}$ are able to be determined. Herein, reference to Z or Y shall refer to the impedance or admittance at the driving point. The total sound power radiated from the plate due to the force may be determined from the plate velocity, by summing the contributions from the resonant and non-resonant vibration velocities:

$$W_{out,total} = W_{out,resonant\ vibration} + W_{out,non\text{-}resonant\ vibration}$$

The resonant vibration component of the total radiated sound power may be determined from the average resonant vibration velocity in the plate which can be estimated from the plate response at the driving point by accounting for the plate properties, namely it's mass and damping. Cremer et al [7] derive an average resonant vibration velocity by considering the vibration resonances or modes of the plate and assuming that at least five modes are contained within any frequency interval of interest, a condition which is more readily satisfied when the wavelength being considered is small relative to the lateral dimensions of the plate. From discussions in Cremer et al [7] it can be shown that:

$$< v^2 > = \frac{W_{in}}{\omega \eta \rho_S S} = \frac{< F_p^2 Y >}{\omega \eta \rho_S S} \qquad (3)$$

Where $\omega = 2\pi f$ is the angular frequency, $\eta$ is the total loss factor which describes the damping losses, $\rho_s$ is the mass per unit area (kg/m$^2$) or surface density of the plate with density $\rho$, S is the surface area (m$^2$) of the plate and $W_{in}$ is the sound power input to the plate from the point force. Vigran [10] presents the following equation where $<v^2>$ can be used to calculate the sound power generated from the plate's reverberant vibration field

$$W_{out,resonant\ vibration} = < v^2 > \cdot \rho_0 c_0 S \sigma \qquad (4)$$

Where $\rho_0$ and $c_0$ are the density of air and the speed of sound in air respectively and $\sigma$ is the radiation efficiency. The product, $\rho_0 c_0$ is often referred to as the characteristic impedance.

For materials with a relatively high bending stiffness, such as concrete, it is generally sufficient to consider only the resonant vibration velocity when determining the sound power generated by a point force. However, the non-resonant vibration component of the radiated sound power may be easily determined and it becomes more relevant when considering light weight plates with relatively lower bending stiffness and relatively more damping or, in other words, plates with a less significant resonant vibration field. The non- resonant vibration component of the total radiated sound power may be evaluated as the power radiated from a point force excitation of (forced) bending waves on an infinite thin plate as described by Cremer et al [7]. Where the force is centred on the driving point and the resulting plate vibrations decrease with increasing distance

away from the driving point, the radiated sound power may be described directly in terms of the force without explicitly considering the plate velocity:

$$W_{out,non-resonant\ vibration} = \frac{F_p^2 \rho_0}{2\pi\rho_S^2 c_0} \tag{5}$$

Vigran [10] notes that eqn (5) is valid where the wave number of the bending wave is much greater than the wave number in air. In this paper eqn (5) is applied below the critical frequency. It is worth noting that eqn (5) does not explicitly include either impedance or radiation efficiency. In other words, the sound power radiated from the bending wave near field effectively depends only on the mass of the panel and the input force.

The total radiated sound power may be found by summing (4) and (5). Consolidating eqns (2), (3), (4) and (5) the total radiated sound power may be expressed as follows:

$$W_{out,total} = \frac{< F_p^2 Y > \rho_0 c_0 S \sigma}{\omega\eta\rho_S S} + \frac{F_p^2 \rho_0}{2\pi\rho_S^2 c_0} \tag{6}$$

Once the total radiated sound power has been determined, the sound intensity level radiating from the plate or the sound pressure level in a particular room may be calculated from established theory, as required for evaluation purposes. From eqn (6) $\omega$, $\rho_0$, $\rho_s$, S and $c_0$ are easily determined. The remaining factors $F_p$, Y, $\eta$ and $\sigma$ warrant further consideration and are discussed in more detail below. In addition, a brief discussion of ceiling attenuation is also provided.

**2.2 Force**

The discussion in the proceeding section applies generally to a point force. Most commonly, the point force considered in the texts ([6], [7]) is the impact of a hammer of a standard tapping machine. Though a tapping machine comprises five hammers it is sufficient to initially consider the excitation from one hammer drop and to then scale the result according to the number of hammer drops which occur in one second. Analogously, for rain noise it is sufficient to initially consider the excitation from a single rain drop and thereafter scale the result according to the cumulative impact of many rain drops, or in other words of rainfall, on a plate.

The impact of a liquid drop, such as a rain drop, hitting a plate has been well described by Petersson [3], who assumes that a drop is spherical in shape at the start of its descent and notes that the shape distorts as the drop falls, with the base of the drop becoming flatter. When the drop impacts the plate it will be rapidly decelerated until the forces within the drop exceed the surface tension of the drop causing it to break. Petersson [3] assumes that water from the broken drop will flow outwards from the point of the impact. The force on the plate can be found by the rate of change of momentum of the drop as it is decelerated during impact and as its downward velocity is directed radially outwards.

Because of the flattened shape of a raindrop at the moment of impact the initial deceleration phase will be very short. It is assumed that the second phase, the flow phase, begins immediately [3]. It is also assumed that the vertical velocity of the drop as it flows radially outwards is constant and is the same as the velocity at the moment of impact [3]. The precise shape of a drop at the moment of impact is difficult to determine in practice. To develop the analysis various idealised drop shapes are proposed. Petersson [3] considers two idealised drop shapes: cylindrical-hemispherical, and; paraboloidal. In addition a further idealised, cylindrical drop shape is considered below. The drop shapes are shown graphically in Figure 1.
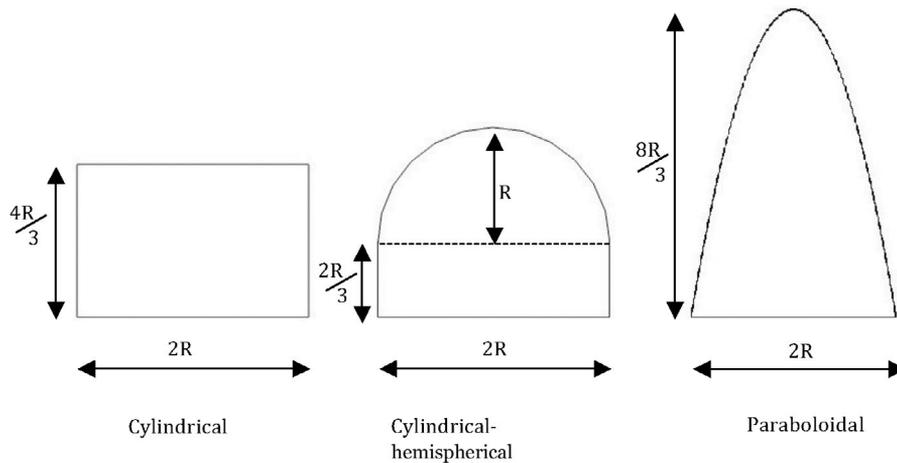


Figure 1.    Idealised drop shapes

The force from a single drop depends on the size or volume of the drop. For an assumed drop shape and a known volume, the radius of the drop may be determined as may its mass. If the drop height is known the velocity of a drop may also be determined. From the mass and velocity Petersson [3] describes the change in momentum with time, that is the force, as follows:

$$F(t) = \frac{d}{dt}(mv) = m\frac{d}{dt}(v) + v\frac{d}{dt}(m) \qquad (7)$$

Here, if the deceleration phase, $m\frac{d}{dt}(v)$, is assumed negligible then the force can be determined from the flow phase, described by $v\frac{d}{dt}(m)$. To carry out an assessment according to eqn (6) the force, F, must be expressed as a function of frequency. Petersson [3] derives the force function for a given drop shape by first determining a mass-time function, which describes the decrease in mass over time due to the water leaving the drop. A force function with respect to time may then be derived according to eqn (7). A Fourier Transform will then provide an expression for the force with respect to frequency. For each of the three drop shapes illustrated in Figure 1, the mass-

time function and resulting force function expressed in terms of frequency are presented in the sections below.

*Cylindrical drop*
The volume ($m^3$) of the initially spherical drop is

$$V_{drop} = \frac{4\pi R^3}{3} \tag{8}$$

where R is the drop's radius (m). Assuming that the volume of the drop remains constant through any changes in shape and that the radius of an idealized cylindrical drop is also R, the height of that cylindrical drop is $4R/3$. Assuming further that the drop velocity during the impact is constant, being equal to the velocity $v_0$ of the drop at the moment of impact and also assuming that the flow phase of the impact begins immediately, the mass-time function for the cylindrical drop is

$$m(t) = \rho_w \pi R^2 \left[\frac{4R}{3} - v_o.t\right] \quad 0 \leq t \leq \frac{4R}{3v_o} \tag{9}$$

Where $\rho_w$ is the density of water. The resulting force function with respect to time can be found from the flow phase change in momentum, $m\frac{d}{dt}(v) = m'(t)v_o$. For the cylindrical drop shape, the force function is a constant over the time interval of interest:

$$F(t) = \rho_w \pi R^2 v_o^2 \quad 0 \leq t \leq \frac{4R}{3v_o} \tag{10}$$

Applying a Fourier Transform

$$F(\omega) = \int_{-\infty}^{\infty} F(t)e^{-j\omega t} \, dt \tag{11}$$

to the force function in eqn (10), the force can be expressed in terms of frequency as follows

$$F(\omega) = \rho_w \pi R^2 v_o^2 \left[\left(\frac{1}{\omega}\right) \sin\left(\frac{4R\omega}{3v_o}\right) + j\left[\left(\frac{1}{\omega}\right) \cos\left(\frac{4R\omega}{3v_o}\right) - \frac{1}{\omega}\right]\right] \tag{12}$$

*Cylindrical-hemispherical drop*

The mass-time function and force functions in the time and frequency domains for a cylindrical-hemispherical drop are described by Petersson [3] as follows, with further details provided in Appendix A.

$$m(t) = \rho_w \pi R^2 \begin{cases} \dfrac{2R}{3} - (h - v_o . t) & v_o . t \leq h \\ \dfrac{2R}{3} + \dfrac{(v_o . t - h)^3}{3R^2} - (v_o . t - h) & h \leq v_o . t \leq h + R \end{cases} \tag{13}$$

Where the height of the cylinder part of the drop, h, is 2R/3. Eqn (15) describes the resulting force function with respect to time, found from the change in momentum:

$$F(t) = \begin{cases} \rho_w \pi R^2 v_o^2 & 0 \leq t \leq \dfrac{2R}{3v_o} \\ -\rho_w \pi R^2 v_o^2 \left[ \dfrac{5}{9} + \dfrac{4v_o t}{3R} - \dfrac{v_o^2 t^2}{R^2} \right] & \dfrac{2R}{3v_o} \leq t \leq \dfrac{5R}{3v_o} \end{cases} \tag{14}$$

Eqn (16) describes the resulting force function with respect to frequency[1].

$$F(\omega) = \rho_w \pi R^2 v_o^2 \left\{ \left[ \left(\dfrac{2}{\omega^3}\right)\left(\dfrac{v_o}{R}\right)^2 \left(\sin\left(\dfrac{5R\omega}{3v_o}\right) - \sin\left(\dfrac{2R\omega}{3v_o}\right)\right) - \left(\dfrac{2}{\omega^2}\right)\left(\dfrac{v_o}{R}\right)\cos\left(\dfrac{5R\omega}{3v_o}\right) \right] \right.$$
$$\left. + j \left[ \left[\left(\dfrac{2}{\omega^3}\right)\left(\dfrac{v_o}{R}\right)^2 \left(\cos\left(\dfrac{5R\omega}{3v_o}\right) - \cos\left(\dfrac{2R\omega}{3v_o}\right)\right) + \left(\dfrac{2}{\omega^2}\right)\left(\dfrac{v_o}{R}\right)\sin\left(\dfrac{5R\omega}{3v_o}\right)\right] - \dfrac{1}{\omega} \right] \right\} \tag{15}$$

*Paraboloidal drop*

For a paraboloidal drop the mass-time function and force function in the frequency domain[1] are described by Petersson [3] as follows, with further details provided in Appendix A.

$$m(t) = \rho_w \pi R^3 \left[ \dfrac{4}{3} - \dfrac{v_o . t}{R} + \dfrac{3}{16}\dfrac{v_o^2 t^2}{R^2} \right] \quad 0 \leq t \leq \dfrac{8R}{3v_o} \tag{16}$$

$$F(\omega) = -\rho_w \pi R^2 v_o^2 \left[ \left(\dfrac{3v_o}{8R\omega^2}\right)\left(1 - \cos\left(\dfrac{8R\omega}{3v_o}\right)\right) - \dfrac{j}{\omega}\left[1 - \left(\dfrac{3v_o}{8R\omega}\right)\sin\left(\dfrac{8R\omega}{3v_o}\right)\right] \right] \tag{17}$$

---

[1]The equation differs slightly from that presented in [3], which may have suffered a printing error.

*Comparison of drop shapes*

A comparison of the three different drop shapes is presented below for a single drop with a diameter of 5mm and an impact velocity of 7m/s which is consistent with the characteristics of Heavy rain according to ISO140-18 [1]. The time history of the impact for each drop shape is shown in Figure 2.
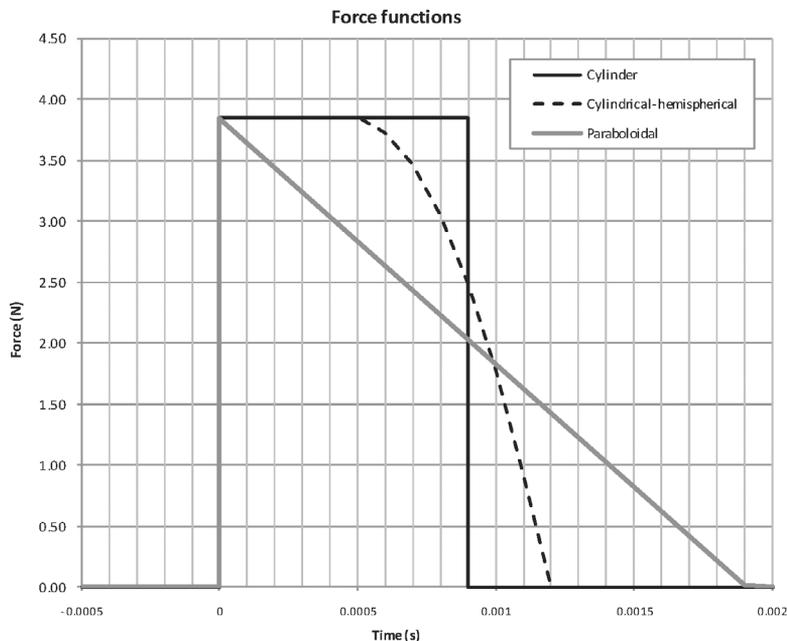


Figure 2.      Comparison of force functions with respect to time

The initial peak of the force is the same in all cases, $\rho_w \pi R^2 v_o^2$. The cylindrical drop has the shortest impact duration, $t = \frac{4R}{3v_o}$, and its time history is in the form of a step function. The time history of the cylindrical-hemispherical drop is initially the same as the cylinder shape drop, until the transition to the hemispherical section of the drop, where the force begins to fall off gradually such that the impact duration is slightly longer, $t = \frac{5R}{3v_o}$. The paraboloidal drop shape has a linear decay with time and has the longest impact duration, $t = \frac{8R}{3v_o}$. The consequences of the differing impact duration can be seen in Figure 3 which shows the variation in force with respect to frequency. For all drop shapes the force spectrum is constant in the low frequency region.  .
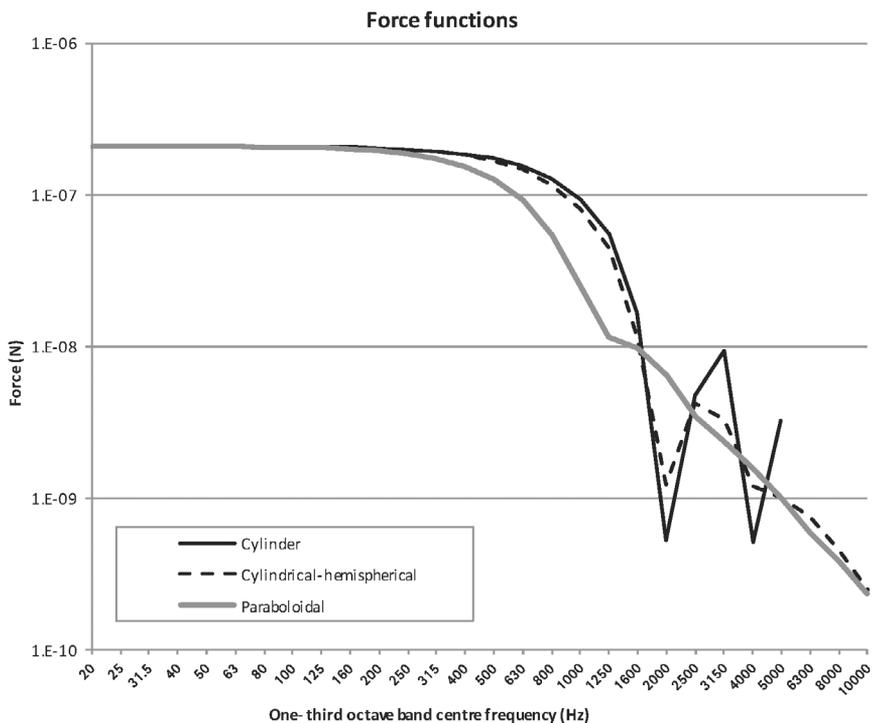
Figure 3.        Comparison of force functions with respect to frequency

The cut-off frequency, below which the force spectrum is constant, is determined by Petersson [3] as:

$$f_{cut\ off} = \frac{1}{2\pi}\left(\frac{v_0}{2R}\right) \qquad (18)$$

For the current example, the cut-off frequency is approximately 111Hz. Above the cut-off frequency, the paraboloidal drop falls away most rapidly with increasing frequency. The spectra of the cylindrical and cylindrical-hemispherical drops are very similar with the cylindrical drop having more pronounced harmonics. The paraboloidal drop will be used in subsequent analysis discussed in this paper.

*Rainfall types*
A discussion of rainfall types is provided in Appendix B.

**2.3 Impedance and admittance**
A model for the system impedance of a rain drop impacting on a plate should generally consider the impedance of both the plate and the drop, as described by Hopkins [2]:

$$Z_{system} = Z_{drop} + Z \qquad (19)$$

For plate materials with high impedance, such that $Z \gg Z_{drop}$, $Z_{drop}$ has little influence on $Z_{systems}$ and the model can often be simplified by ignoring it. Drop impedance becomes more significant for light weight plates such as plywood which have a relatively low impedance when compared with, for example, concrete.

*Drop impedance*
Petersson [3] describes the impedance of a rain drop as follows

$$Z_{drop} = \frac{1}{Y_{drop}} = \rho_w \pi R^2 v_0 \tag{20}$$

Where the drop impedance is significant, the resulting driving point velocity of the plate will decrease.

*Infinite plate impedance*
The driving point impedance of an infinite, homogeneous, isotropic plate for the excitation of bending waves has been described by Hopkins [2] as:

$$Z = 8\sqrt{\rho_s B} \tag{21}$$

Hassan [9] notes that eqn (21) is valid for thin plates, such that the thickness is smaller than a sixth of the bending wavelength. Expressed as mobility it may be written:

$$Y = \frac{1}{8\sqrt{\rho_s B}} \tag{22}$$

In the above, B is the bending stiffness of the thin plate, which Hopkins [2] describes as:

$$B = \frac{Eh^3}{12(1 - v^2)} \tag{23}$$

where E is Youngs Modulus (Pa), h is the plate thickness (m) and $v$ is Poisson's ratio, which is approximately 0.3 for most roofing materials. It can be observed from eqns (21) and (22) that the impedance/admittance for an infinite plate is real and is independent of frequency.

An alternative expression for the admittance can be derived as a function of the longitudinal wave speed. Where longitudinal wave speed, $c_L$ is estimated by Cremer et al [7] as:

$$c_L = \sqrt{\frac{E}{\rho(1 - v^2)}} \tag{24}$$

combining eqn (23) and (24) the following equation can be determined:

$$Y = \frac{1}{2.3 \rho c_L h^2} \qquad (25)$$

Eqn (25) allows calculation of admittance for an infinite plate using the plate's thickness and the plate material's longitudinal wave speed. This is often helpful as the longitudinal wave speed for many materials is available in the literature and it would avoid having to directly consider the Youngs Modulus. However, the assumptions used to derive eqn (25), namely that the plate is thin and infinite, mean it tends to be less accurate at extremes of the frequency range.

*Finite plate impedance*
The infinite plate equations discussed above provide a good approximation for a finite plate where the wavelength being considered is very small relative to the width and length of the plate. In fact, the impedance equation for an infinite thin plate, eqn (22), also represents the average or mean impedance of a finite plate, when averaged over all input points and over the frequency band of interest [10].

However, for a finite plate, such as would be used in a rain noise measurement, the admittance will be influenced by the modal response of the plate, particularly in the mid and low frequency regions, such that the average response will not be sufficiently representative of the modal peaks. Also, the low frequency impedance of light weight test panels is likely to be controlled by the joists of the support frame rather than the test panel itself [11].

For simplicity the current analysis assumes impedance behaviour of an infinite plate. This assumption will lead to relatively greater prediction errors at low frequencies

*Orthotropic panels*
As noted, the discussion of driving point impedance is valid for isotropic materials. A need can often arise to consider orthotropic plates, for example roofing materials such as corrugated iron, which can have significantly different bending stiffness parallel and perpendicular to the corrugations. Orthotropic plates can often be approximated by an isotropic plate by considering the effective bending stiffness of the plate, as described by Hopkins [2]:

$$B_{eff} = \sqrt{B_x B_y} \qquad (26)$$

Where $B_x$ and $B_y$ are the bending stiffness in the x and y (orthogonal) directions respectively.

For simplicity, the analysis in this paper assumes isotropic panels for all plates considered.

*Surface impact*
The analysis detailed in this paper assumes that each drop impacts directly onto the test plate. In practise, after a brief period of constant rainfall the test plate will be covered with a thin layer of water meaning that subsequent drops will impact on the water layer

rather than directly onto the test plate. Petersson [3] notes that where a drop impacts on a wet surface the impact peak is reduced and the pulse duration is extended. The frequency characteristics of the force are therefore diminished at high frequencies. This is a cause of uncertainty in the prediction model.

### 2.4 Damping

The damping term, $\eta$, in eqn (6) is the total loss factor which represents all energy losses from the plate which balance the input vibration velocity and result in the given resonant vibration velocity for the plate. These losses can be due to a number of causes including internal losses within the plate due to conversion of vibration energy to heat [2], edge losses at the plate perimeter as the vibration energy is transferred to a surrounding structure and losses due to sound radiation into the surrounding air. Considering these factors separately the total loss factor can be expressed as

$$\eta_{total} = \eta_{flanking} + \eta_{rad} + \eta_{int} \tag{27}$$

Each component of the total loss factor is considered below.

*Radiation losses*

In most cases, energy losses due to radiation are so small that they may be neglected. However, this is not universally the case. Losses due to radiation are described by Craik [8] using a statistical energy analysis (SEA) approach and can be expressed as follows

$$\eta_{rad} = \frac{\rho_0 c_0 \sigma}{\omega \rho_S} = \frac{\rho_0 c_0 \sigma}{2\pi f \rho_S} \tag{28}$$

At frequencies below the critical frequency the radiation efficiency is typically so small as to render the radiation damping negligible. Similarly at frequencies above the critical frequency, where $\sigma \approx 1$, the frequency component in the denominator of eqn (28) will often render the radiation damping negligible. However, in some cases the radiation damping in the region of the critical frequency, where $\sigma > 1$ and f is sufficiently small, can be significant and is therefore worth considering as part of the total loss factor. In eqn (28) the value of $\sigma$ relates to radiation from one side of the plate only. To estimate the radiation losses due to radiation from both sides for the plate, the fraction on the right hand side of eqn (28) should be multiplied by 2.

*Flanking losses*

Flanking losses, that is losses at the edge of the test plate where energy is transferred to the surrounding structure, will vary depending on the properties of the test plate and those of the surrounding structure. EN 12354-1 [12] describes an expression for the total loss factor which includes consideration of flanking losses in a laboratory situation where the surrounding structure is relatively massive. Equation (C.5) of [12] states:

$$\eta_{tot,lab} = \eta_{int} + \frac{\rho_S}{\left(485\sqrt{f}\right)} \qquad (29)$$

Where $\eta_{int}$ is the internal damping, as discussed below. While the laboratory setting is rather particular, the total loss factor in eqn (29) provides reasonable prediction accuracy for more general predictions of field settings. In particular it provides a simple and concise expression for the total loss factor, which includes a dependence on frequency. The expression does not explicitly consider radiation losses, though this can be included via the discussions above.

*Internal losses*
Internal losses account for energy losses due to internal friction. They are also often assumed to account for any other sources of energy loss which have not been explicitly considered in the prediction model. Typically internal losses are assumed to be independent of frequency. Example values are presented in Table 1, sourced from Hopkins [2].

**Table 1. Indicative values for damping**

| Material | Internal damping |
|---|---|
| Concrete | 0.005 |
| Plywood | 0.016 |
| Steel | $\leq 0.0001$ |

Hopkins [2] notes that the assumption of a frequency independent internal loss factor is reasonable for solid, homogeneous materials for the building acoustics frequency range but that some materials can exhibit frequency dependent damping, in particular with damping which increases with increasing frequency such as laminated glazing. Our subsequent analysis in this paper will assume a frequency independent internal loss factor, and the uncertainty associated with this should be noted.

*Comments*
The rain prediction model presented herein is reasonably sensitive to changes in damping. As shown in eqn (6) the resonant vibration velocity component of the total radiated sound power is directly proportional to $1/\eta$. Where the resonant vibration velocity dominates the total radiated sound power, as typically occurs for rain noise, a doubling of the damping will decrease the radiated sound power by a half (a 3dB decrease in sound power level).

**2.5 Radiation Efficiency**
In eqn (6) the radiation efficiency is incorporated into the resonant vibration velocity component of the total radiated sound power. For a finite plate with a given resonant vibration velocity, expressions for the average radiation efficiency for a simply

supported plate have been derived by Maidanik [13] and are well described in most reference texts [6], [8], [2].

For light weight plates which are supported by joists, there may be some reduction in vibration velocity at each junction with a joist meaning that the vibration in the plate is not well described by the idealized resonant vibration velocity which is assumed to be constant over the entire plate. This variation in velocity may effect the resulting predictions of radiation efficiency which, for a finite plate, necessarily consider the plate dimensions and assume an average velocity over the entire plate. This is a cause of uncertainty in the prediction model.

It can also be observed that the non-resonant vibration velocity component of radiated power, eqn (5) does not explicitly include a radiation efficiency term.

### 2.6 Ceiling Effects

Eqn (6) may be used to determine the sound power radiated from a single plate. Theory developed by Sharp [14] may be used to examine the effects of installing a ceiling beneath the plate. It is advantageous to consider the airborne and structure born paths through the ceiling separately.

*Airborne path*

Sharp [14] describes a model for transmission loss through a double panel partition where the two panels are separated by a cavity which is without structural connections but includes some sound absorptive material. Sharp's model is developed from consideration of infinite, thin panels such that the panel lateral dimensions are much greater than the bending wavelengths being considered. Concurrently, it is assumed that any standing waves in the air cavity are sufficiently damped by the sound absorptive material such that the air contained in the cavity acts as a stiffness element. Equation (6) from Sharp's paper details a relationship between the transmission loss (based on the mass law) of the elements and the transmission loss of the overall partition, as follows:

$$\text{TL} = \begin{cases} \text{TL}_M & f < f_0 \\ \text{TL}_{m_1} - \text{TL}_{m_2} - 20\log(fd) + 29 & f_0 < f < f_1 \\ \text{TL}_{m_1} - \text{TL}_{m_2} - 6 & f > f_1 \end{cases} \tag{30}$$

Where $\text{TL}_{m_1}$ and $\text{TL}_{m_2}$ are the mass law transmission losses of the first and second panels of the partition respectively, $M = m_1 + m_2$ and d is the separation between the two panels (m). $f_1$ is equal to 55/d and $f_0$ is the mass-air-mass resonance of the panel-cavity-panel system and is given by $113/\sqrt{m_e d}$ where Sharp describes $m_e$ as follows:

$$m_e = \frac{2m_1 m_2}{(m_1 + m_2)} \tag{31}$$

To estimate the effect of a ceiling suspended below a roof, we can re-arrange Sharps equation, calculating $\text{TL} - \text{TL}_{m_1}$ to determine the influence of the air cavity and ceiling

panel. Applying this effect to the sound power level radiated from the roof, $L_{w,out,total} = 10\log_{10}\left(\frac{W_{out,total}}{w_{ref}}\right)$, we get an expression for the sound power level radiated from the ceiling:

$$L_{W,Ceiling,Air} = \begin{cases} L_{W,out,total} - \Delta TL_M & f < f_0 \\ L_{W,out,total} - TL_{m_2} - 20\log(fd) + 29 & f_0 < f < f_1 \\ L_{W,out,total} - TL_{m_2} - 6 & f > f_1 \end{cases} \quad (32)$$

Where, $L_{W,Ceiling,Air} = 10\log_{10}\left(\frac{W_{Ceiling,Air}}{w_{ref}}\right)$ and $W_{ref} = 10^{-12}$ W..

In the very low frequency region it may be assumed that the roof/ceiling system behaves as a lumped mass. Accordingly, $\Delta TL_M$ is the difference between the mass law transmission loss of the first panel $TL_{m_1}$ and the combined mass law transmission loss $TL_M$ of the test plate and the ceiling when treated as an equivalent single plate such that:

$$\Delta TL_M = TL_M - TL_{m_1} \quad (33)$$

*Structure borne path*

Where there are structural connections between the test plate and the ceiling, as can regularly occur in practice due to the presence of joists and wire hangers in a roof/ceiling installation, the connections will reduce the transmission loss gains described above. Assuming that the ceiling lining is sufficiently damped for the effect of the structural connection to be controlled by non-resonant radiation, Cremer et al [7] provide an expression for the radiated sound power due to line connections:

$$W_{Ceiling,structure} = \frac{2\rho_0 c_0 n l \lambda_c < v_{Connection}^2 >}{\pi} \quad (34)$$

Where $n$ is the number of line connections, of length $l$ (m) and $\lambda_c = c_0/f_c$ is the wavelength at the critical frequency of the ceiling lining. $<v_{Connection}^2>$ is the non-resonant vibration velocity of the ceiling panel at the line connection.

Where $v$ is the vibration velocity of the test plate (roof) and $v_{bridge}$ is the vibration velocity of the structural connection, Sharp [14] provides as expression for the force induced in the structural connection from the test plate:

$$F_{bridge} = Z_1(v - v_{bridge}) \quad (35)$$

Where $Z_1$ is the impedance of the roof plate as seen by the line connection. Where $v_{Ceiling}$ is the velocity of the ceiling without the contribution of $v_{Connection}$, the force induced in the bridge can similarly be described as:

$$F_{bridge} = Z_2\left(v_{bridge} - v_{Ceiling}\right) \tag{36}$$

Where $Z_2$ is the impedance of the ceiling plate as seen by the line connection. If it is assumed that the structural connection is rigid and massless, that $v_{Connection} = v_{bridge}$ and $v_{bridge} \gg v_{Ceiling}$ then the following relationship between v and $v_{Connection}$ may be derived, as detailed by Equation (16) of Sharp's paper:

$$\frac{v}{v_{Connection}} = (Z_1 + Z_2)/Z_1 \tag{37}$$

Where the line connection impedances $(Z_1, Z_2)$ can be determined from $Z = 2(1 + j)\rho_S c_0 \sqrt{f/f_c}$. Eqn (34) and eqn (37) can be rearranged to provide the following expression for the sound power radiated from the structural connections:

$$W_{Ceiling,structure} = \left(\frac{2\rho_0 c_0 n l \lambda_c}{\pi}\right) < v^2 > \left((Z_1)/(Z_1 + Z_2)\right)^2 \tag{38}$$

An adjustment of $W_{Ceiling,structure}$ may be made for frequencies below $f_0$, as outlined for the airborne case above, in order to account for the combined mass of the roof and ceiling plates in the very low frequency region.

The combined effect of airborne and structure borne paths through the ceiling may be determined as:

$$W_{Ceiling} = W_{Ceiling,Air} + W_{Ceiling,structure} \tag{39}$$

## 3.0 MEASUREMENTS
### 3.1 Measurement arrangements
The results of a small series of measurements of artificial rain noise are presented herein. The measurements were carried out in 1993 but were not published at that time. As the measurements were carried out prior to the release of ISO140-18, the characteristics of the artificial rain generated differ from the standard. Details of the measurement arrangements are outlined below.

A small rig, shown schematically in Figure 4, was constructed to generate rain drops with known characteristics and to enable the acoustical response of test roofs to be measured accurately.

A one square metre test roof and frame were placed on a simple stand to permit easy access to the underside of the roof. The stand was designed to give a 5° pitch to the roof and a simple gutter on one side collected the water and directed it into a bucket. The roof frame sat on a 10 mm thick pad of foam plastic to prevent vibration being transmitted into the stand.
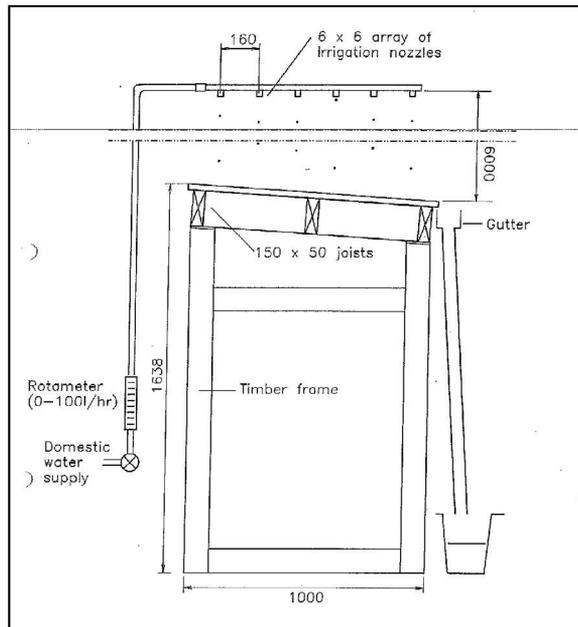
Figure 4.        Measured damping levels

Rain was simulated with constant sized drops from an array of 36 irrigation nozzles. Water from an ordinary domestic tap was supplied to the rain maker via a flow meter. This allowed precise control of the water flow to the rain maker and rapid adjustment to the required rain fall rates.  The drop diameter was determined by measuring the volume of a known number of drops through one nozzle and assuming that all drops are of equal volume.

The drops had an equivalent diameter (for a spherical drop shape) of 5.8 ± 0.3 mm at 30 mm/hr rain fall. The mean drop diameter increased slightly with flow rate. Individual nozzles in the array were adjusted so that the flow rates were within ± 20% of the mean.  At the maximum flow rate of 70 l/hr, equivalent to a 70mm/hour rainfall rate for the $1m^2$ test plates, there were about 5 drops per second from each nozzle and 190 drops per second from the overall array. The drops fell a height of 6.0 m to hit the test roof.

The noise generated by the impact of the rain drops was measured by scanning the underside of the roof with a sound intensity probe.  The intensity was measured in 1/3 octave bands from 100Hz to 5kHz.

Each roof material was fixed in accordance with normal practice to a roof frame consisting of 150 mm x 50 mm timber joists at 500 mm centres. The rain maker was adjusted to give the required rainfall rate.  As noted in Appendix B, the rainfall in this apparatus does not necessarily represent natural rainfall of the same rate since the raindrops are all of one specific size, whereas in natural rain the drops would be distributed over a range of sizes and would be travelling at different velocities

depending on size. Ballagh [4] notes that a large proportion of drops in natural rainfall are small and do not contribute significantly to the noise. Comparing our results with Dubout's [15] measurements of natural rain fall on comparable roof constructions, the noise generated from the 70mm/hr artificial rain, comprising approximately uniform large drops, is much higher than a natural rainfall of 70mm/hr and is estimated equivalent to a natural rainfall of approximately 300mm/hr.

Initial tests were conducted to determine the performance of the system using a bare corrugated steel roof. The average sound intensity was measured at various flow rates from 10mm/hr to 70mm/hr. As expected the noise level increased by about 10 dB per 10 fold increase in rainfall rate. Note that with natural rainfall the noise will increase by 17 dB per 10 fold increase in rainfall rate because the proportion of larger drops which have a higher terminal velocity increases at higher rainfalls [4]. Subsequent tests on other roofs used only the maximum flow rate of 70mm/hr.

As well as the sound intensity measurements on each roof type, the damping of each roofing material was measured while the material was mounted on the frame. An accelerometer was placed at several different positions on the roof and the roof structurally excited with a light tap from a hammer. The decay of vibration energy was recorded and the decay rate and damping coefficients were calculated in 1/3 octave bands between 100Hz and 5kHz according the equation B.1 of ISO140-18.

### 3.2 Results

Five different roofing materials were tested. These are described below and shown in Figure 13 in Appendix C.

1.  Corrugated steel 0.55 mm thick with a factory applied paint finish (Custom Orb)
2.  Corrugated fibre cement, 7 mm thick (Hardies Super Six)
3.  Trough section steel, 0.5 mm thick with a factory applied paint finish. (Dimondek 400).
4.  Corrugated glassfibre reinforced plastic, 1.5 mm thick (Glasslite)
5.  Plywood (17.5 mm thick) with 1 mm thick Butynol membrane adhered to the top surface.

In addition one test was carried out on the Plywood roof with a 13 mm thick plasterboard lining nailed to the underside of the roof frame. A blanket of 100 mm thick wool (9kg/m$^3$) was placed in the joist cavity for this test.

The sound intensity levels for each roof material, at an artificial rainfall rate of 70mm/hr, are given in Figure 5. The noisiest roof was the trough section steel with the corrugated plastic roof only slightly quieter. The Fibre Cement roof was the quietest with the Plywood and Butynol roof somewhat noisier. The corrugated steel was intermediate between these.

The measured damping coefficients as a function of frequency are shown in Figure 6. These are measured with the roofing materials fixed to the roof frame. The plywood and butynol roof was the most heavily damped with the corrugated plastic and corrugated fibre cement sheet slightly less damped. The trough section steel was considerably less damped than all other materials.
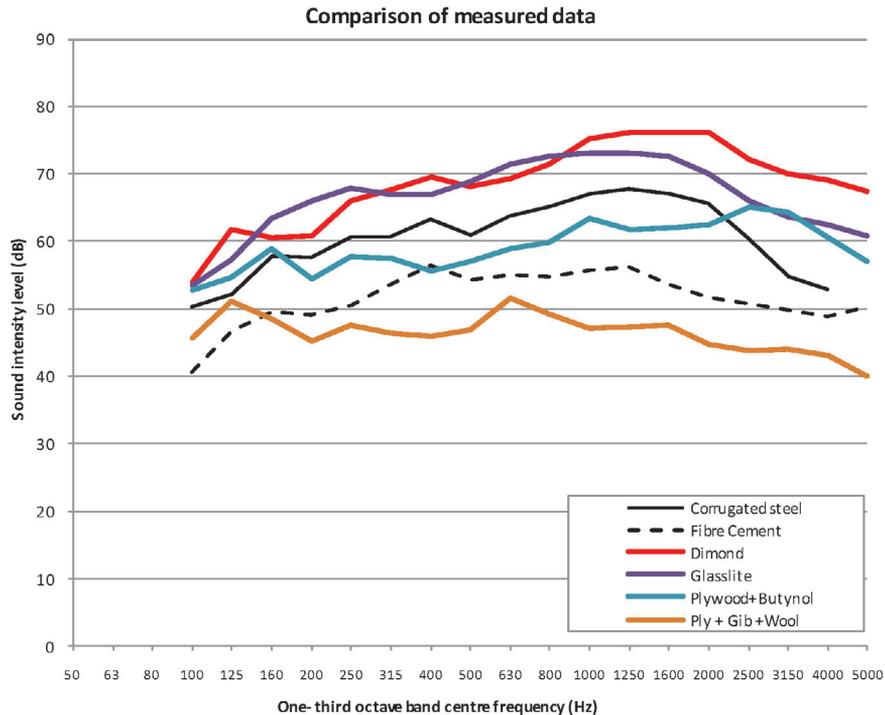
Figure 5.        Measured sound intensity levels for artificial rainfall, 70mm/hr

The measured damping values range from approximately 0.001 to 0.1 depending on material and frequency.  Given that the resonant vibration component of the radiated sound power level is proportional to $1/\eta$, this range of damping values corresponds to a variation of $10^2$ or, in decibel terms, a variation in sound power level of 20dB.  Given the difficulties in establishing the actual damping of a particular installation, and the variation that is likely to occur from test sample to test sample, the damping is a significant source of uncertainty for the prediction model.

Figure 7 through Figure 11 present a comparison of the measured sound intensity for each roof with two sets of predicted results based on eqn (6).  One set of predictions is entirely theoretical, denoted 'predicted', while the other incorporates the measured damping levels in lieu of the theoretical total loss factor outlined earlier.

The overall agreement between measured and predicted sound intensity levels is reasonable, although there can be significant variations at some 1/3 octave bands. There is an observable trend that the measured values are greater than predicted values in the high frequency region, above 500-1000Hz.  This may be due to several factors:

• Force uncertainty, in particular the assumed drop shape may not be sufficiently representative nor may be the assumption that the drops are falling on a dry surface.
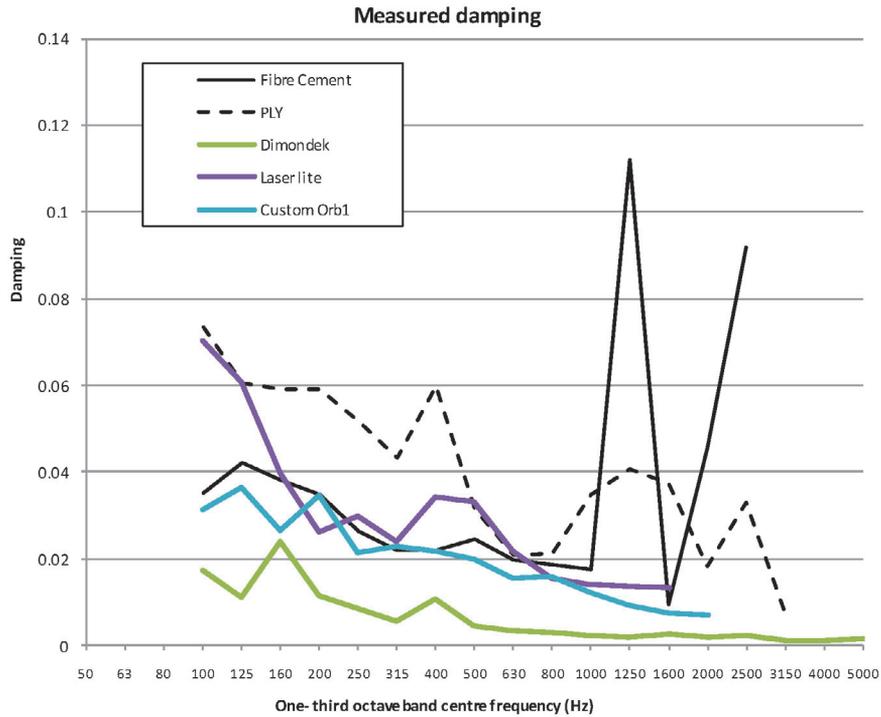
Figure 6.      Measured damping levels

- Impedance uncertainty, specifically the model for impedance of an infinite plate may not be sufficiently representative.
- Uncertainty associated with the critical frequency of the materials.  In particular, the predictions assume the plate material is thin, homogeneous and isotropic.  In practice several of the materials are profiled (corrugated, troughed) and this is likely to introduce a double critical frequency trend including at least one critical frequency which is below that of the equivalent flat plate.

It can also be observed that the predictions based on measured damping generally are in better agreement with measured sound intensity levels.
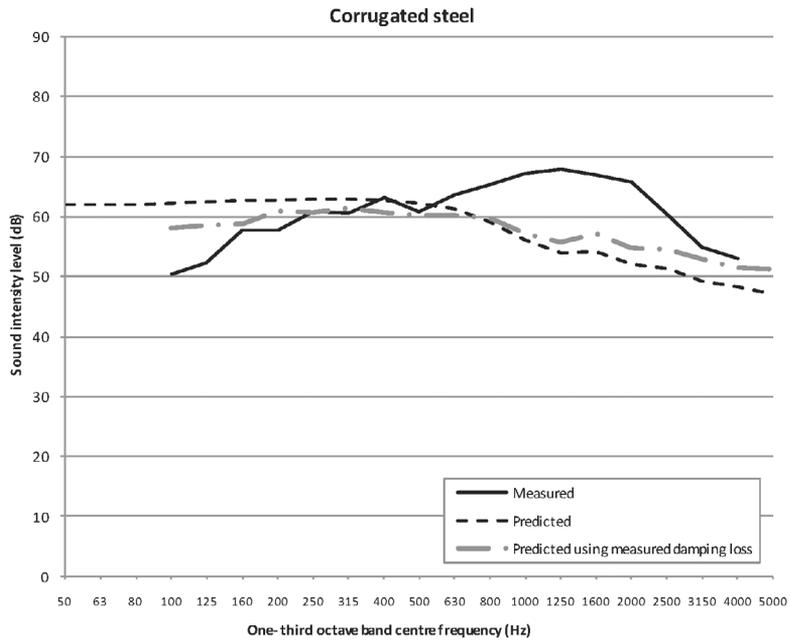
Figure 7.        Measured sound intensity levels, Corrugated steel
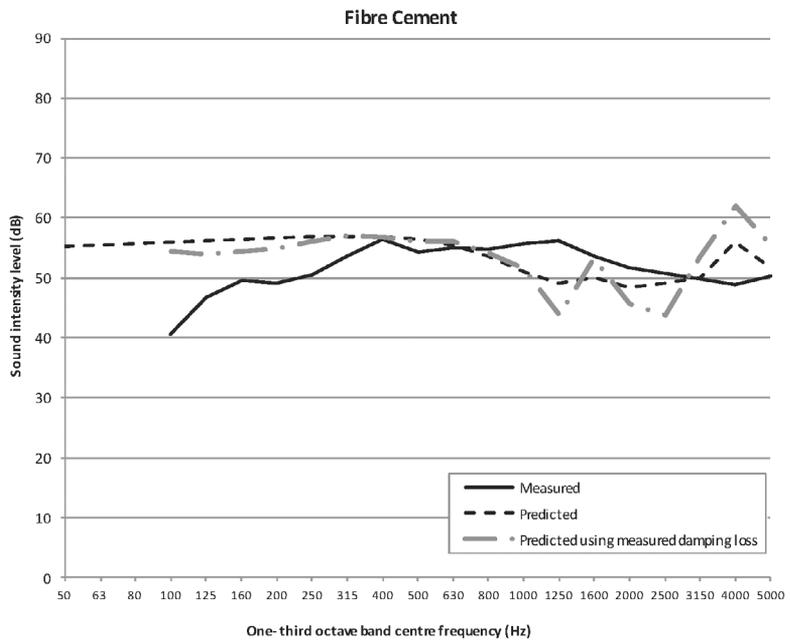


Figure 8.        Measured sound intensity levels, Corrugated fibre cement
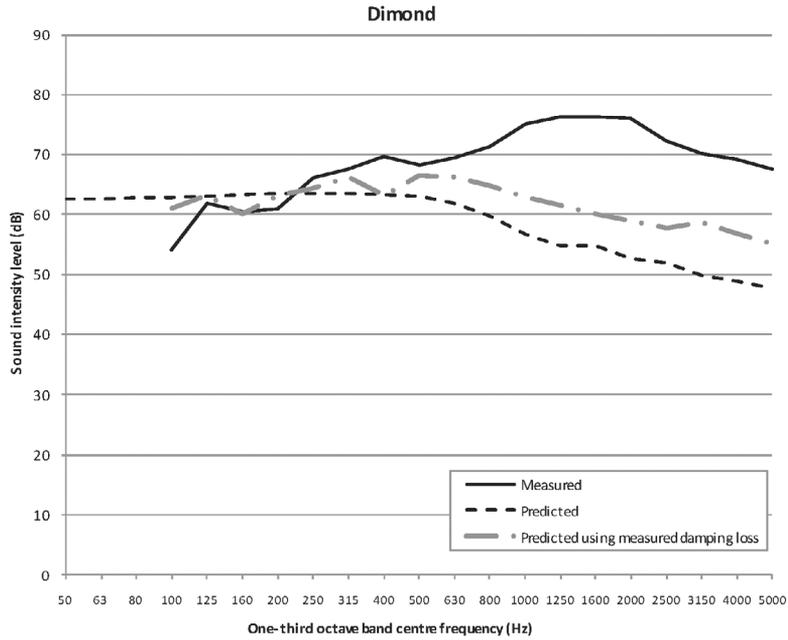
Figure 9.        Measured sound intensity levels, trough section steel
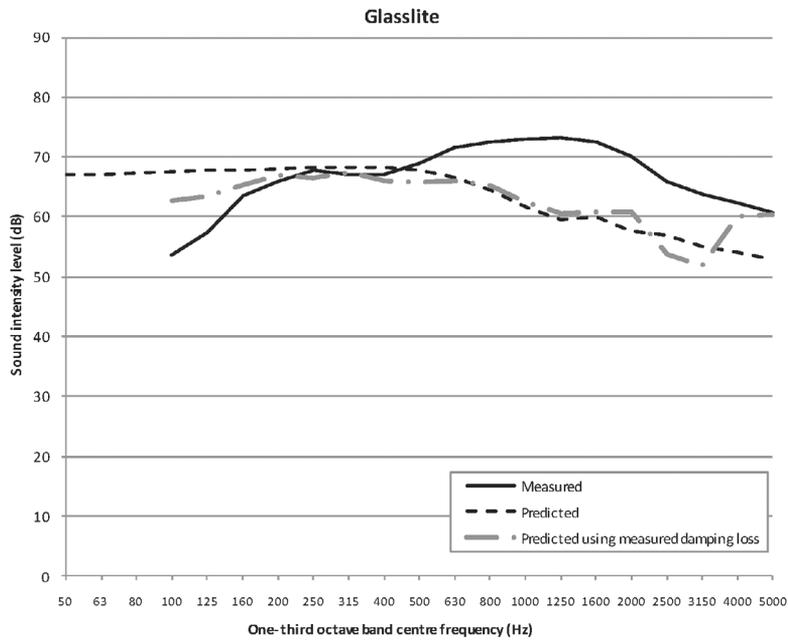


Figure 10.       Measured sound intensity levels, Corrugated glass lite

**Plywood+Butynol**
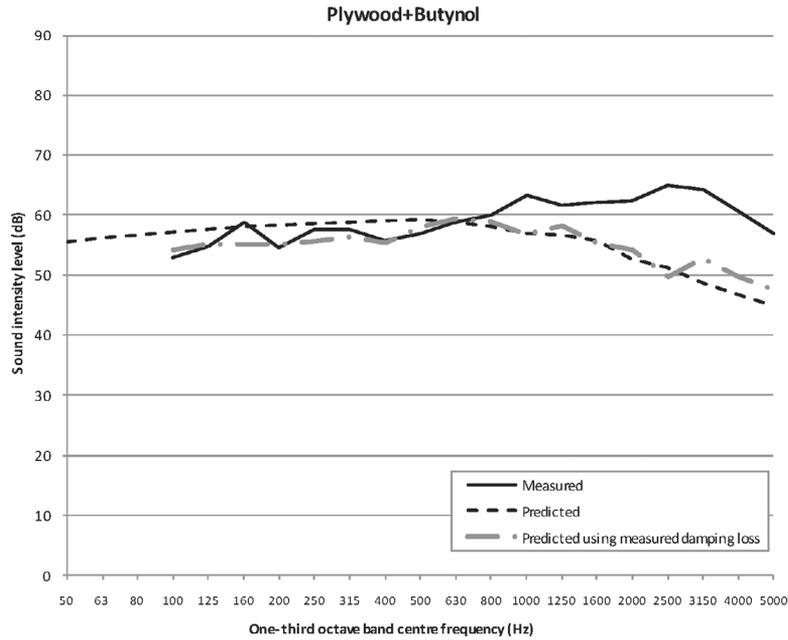
Figure 11.    Measured sound intensity levels, Plywood

The reduction in noise when the plasterboard ceiling was fixed to the underside of the plywood test plate and frame is shown in Figure 12.  It can be seen that there is again reasonable agreement between measured and predicted sound intensity levels.

**Ply + Gib + Wool**
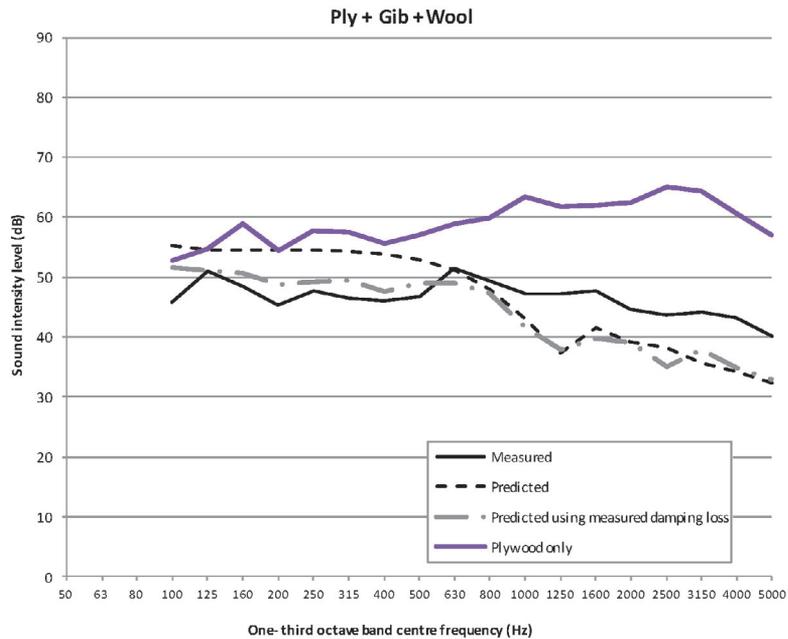
Figure 12.    Measured sound intensity levels, Plywood + GIB

A summary of the measured and predicted A-weighted sound intensity levels is presented in Table 2.

**Table 2. Comparison of measured and predicted levels of rain noise**

| A-weighted sound intensity level (dB re $10^{-12}$ watts/m$^2$) | | | |
|---|---|---|---|
| Construction | Measured | Predicted | Predicted, using measured damping loss |
| Corrugated steel | 75 | 68 | 68 |
| Fibre cement | 64 | 64 | 66 |
| Dimond | 84 | 68 | 73 |
| Glasslite | 81 | 73 | 73 |
| Plywood + Butynol | 73 | 66 | 66 |
| Plywood + Gib + Wool | 57 | 57 | 54 |

## 4.0 CONCLUSION

A theory for rain noise prediction has been presented, based on consideration of the force of one drop on a plate with extension to multiple drops, or rainfall, on a roof. The presented theory provides a reasonably robust engineering model which does not rely on expensive computational techniques or lengthy computer simulation. Comparisons with measured data show reasonable agreement with predicted levels and several possible causes for discrepancies are nominated. Exploring these possible causes would be the next step in any further works.

## REFERENCES

[1]  International Standard 140-18:2006 Acoustics - Measurement of sound insulation in buildings and of building elements - Part 18: Laboratory measurement of sound generated by rainfall on building elements

[2]  Hopkins, C. *Sound insulation*, Butterworth-Heinemann, Oxford, 2007

[3]  Petersson, B.A.T., The Liquid drop impact as a source of sound and vibration, *Building Acoustics*, 1995, 2(4), 585-623.

[4]  Ballagh, K.O., Noise of simulated rain on roofs, *Applied Acoustics*, 1991, 31, 245-264.

[5]  McLoughlin, J., Saunders, D.J., Ford, R.D., Noise generated by simulated rainfall on profiled steel roof structures, *Applied Acoustics*, 1994, 42, 239-255

[6]  Beranek, L. *Noise and vibration control*, McGraw Hill, New York, 1971

[7]  Cremer, L., Heckl, M., Petersson, B.A.T., *Structure-borne sound: Structural vibrations and sound radiation at audio frequencies*, Springer, Berlin, 2005

[8]  Craik, R.J.M., *Sound transmission through buildings using statistical energy analysis*, Gower, Aldershot, 1996

[9]    Hassan, O.A.B., *Building acoustics and vibration - Theory and practice*, World Scientific Publishing Co. Pte Ltd, Singapore, 2009

[10]   Vigran, T.E. *Building Acoustics*, Talyor & Francis, Oxon, 2008

[11]   Fischer, H., Gibbs, B., Mayr, A.R., Spatial variation of the point mobility of a timber joist floor, *Proceedings of DAGA 2008*,

[12]   EN 12354-1:2000 Building acoustics - Estimation of acoustic performance of building from performance of elements - Part 1: Airborne sound insulation between rooms.

[13]   Maidanik, G., Response of ribbed panels to Reverberant Acoustic fields. *Journal of the Acoustical Society of America*, 1962, 34, 809-826.

[14]   Sharp, B.H., Prediction methods for the sound transmission of building elements, *Noise Control Engineering*, 1978, 11, 53-63

[15]   Dubout, P., The sound of rain on a steel roof, *Journal of sound and vibration*, 1969, 10, 144-50.

[16]   Suga, H. and Tachibana, H.,Sound radiation characteristics of lightweight roof constructions excited by rain, *Building Acoustics*, 1994, 1(4), 249-270.

[17]   Marshall, J.S. and Palmer, W.M., The distribution of raindrops with size, *Journal of Meteorology*, 1948, 5, 165-166.

[18]   Best, A.C., Empirical formulae for the terminal velocity of water drops falling through the atmosphere, *Quarterly Journal of the Royal Meteorological Society*, 1951, 76, 302-311

## APPENDIX A

### DROP MASS-TIME FUNCTIONS

*Cylindrical-hemispherical drop*

Petersson [3] determines the following mass-time function equations for a cylindrical-hemispherical drop:

$$m(t) = \rho_w \pi R^2 \left[ \frac{2R}{3} - (h - y(t)) \right] \quad \text{for} \quad y(t) \le h$$

$$m(t) = \rho_w \pi \left[ \frac{2R^3}{3} - \int_0^{(y(t)-h)} (R^2 - \eta^2) d\eta \right] \quad \text{for} \quad h \le y(t) \le h + R$$

Eqn (13) can be derived by calculating the integral and approximating the drop velocity y(t) by $v_0$, the initial velocity of the drop at the moment of impact.

*Paraboloidal drop*

Suga and Tachibana [16] provide an equation for a parabola from which the paraboloidal drop shape can be determined:

$$x^2 = R^2 - \left(\frac{3R}{8}\right)y$$

The mass-time function can then be described as:

$$m(t) = \rho_w \pi \left[\frac{4R^3}{3} - \int_0^{(y(t))} \left(R^2 - \left(\frac{3R}{8}\right)\eta\right) d\eta\right]$$

Eqn (16) can be derived by calculating the integral and approximating the drop velocity $y(t)$ by $v_0$, the initial velocity of the drop, at the moment of impact.

**APPENDIX B**

**TYPES OF RAINFALL**
Natural rainfall comprises a range of drop sizes with a range of drop velocities [17]. This range of drop sizes can be estimated by a statistical distribution as explained below. Prior to this, however, it is worth considering a scenario intermediate between the analysis of one drop, as described above, and analysis of Natural rain. That is artificial rain, as described in ISO140-18, which explains a measurement procedure based on rainfall with a constant drop velocity.

*ISO 140-18 rain types*
Measurements carried out according to ISO140-18 [1] require the use of artificial rain of a known rainfall rate with drops which are approximately constant in size and which fall from a known height above a test plate. The use of a force function comprising a known, constant drop size of a known velocity and a known number of drops means the measurements are more readily reproducible. ISO140-18 describes two different intensities of artificial rain for measurements, with distinct drop sizes and drop velocities as detailed in Table 3.

**Table 3. ISO140-18 rainfall types**

| Type | Rainfall rate (mm/hr) | Typical drop diameter (mm) | Fall velocity (m/s) |
|------|------|------|------|
| Intense | 15 | 2 | 4 |
| Heavy | 40 | 5 | 7 |

To predict the level of rain noise generated by one of the types of artificial rain it is necessary to determine the level of noise generated by one drop of the artificial rain, and then to scale this value by the number of drops per second. The artificial rain is typically generated from a header tank positioned above the test plate, whose base has been perforated with holes sufficient to produce drops of the required size. The portion of the base that is perforated has an area of approximately $1.6m^2$.

Considering heavy artificial rain, for example, with a rainfall rate of 40mm/hr the corresponding rainfall rate per second is

$$\frac{40}{3600} = 0.0\dot{1} \; mm/s$$

To calculate the volume of water which therefore falls from the 1.6m$^2$ header tank in one second it is necessary to correct for the area of the perforated based of the tank. The volume of water falling on the test plate in one second is

$$0.0\dot{1} * 1.6 = 0.0180\dot{5} \; mm^3/s$$

The number of drops which fall onto the test plate in one second can be found by dividing this volume of water by the volume of a single drop. Where the drop diameter is 5mm, the volume of the initially spherical drop is

$$V_{drop} = \frac{4\pi(5)^3}{3}$$

Correcting for units this equates to approximately 276 drops per second falling on the plate during artificial heavy rain. Assuming that the drops are incoherent, the force function for this type of rain can therefore be determined by calculating the force from a single drop of radius 5mm and drop velocity 7m/s and scaling the magnitude of the force by a factor of 276 to account for the number of drops per second.

*Natural rainfall*

Natural rainfall comprises a range of drop sizes. Any given drop will have a particular mass and an associated impact velocity, which can be taken as the terminal velocity of that drop. A prediction model for noise from natural rainfall must address the range of drop sizes, and associated impact velocities and forces, which are likely to occur. The distribution of drop sizes in natural rain can be estimated by an idealized exponential distribution, the Marshall-Palmer distribution [17]. Such a model assumes a degree of temporal and spatial averaging of the natural rainfall. The Marshall-Palmer distribution takes the form

$$N_D = N_0 e^{-\Lambda D} \tag{40}$$

where D is the diameter, $N_D \delta D$ is the number of drops in unit volume of space with a drop size in the range D-(D + $\delta$D) and $N_0$ is the value of $N_D$ for D = 0. Marshall and Palmer give the values of parameters as $N_0$ = 8000m$^3$mm$^{-1}$ and $\Lambda$ = 4.1$\mathbb{R}^{-0.21}$ mm$^{-1}$, where $\mathbb{R}$ is the rainfall in mm/hr.

To use the Marshall-Palmer distribution in practice it is helpful to break up a range of drop sizes into discrete intervals. For example, if a range of drop sizes from 0mm to, say, 6mm is considered, this range can be divided into intervals of, say, 0.1mm.

Consider the interval 5-5.1mm. The Marshall-Palmer distribution will estimate the number of drops within this interval which falls in unit volume of space. The terminal velocity of the drop range may then be determined by a simple empirical formula for the terminal velocity of raindrops in still air as detailed by Best [18]:

$$v_T = 9.58 \left( 1 - \exp\left[ -\left(\frac{D}{0.855}\right)^{1.147} \right] \right) \tag{41}$$

where $v_T$ is the terminal velocity in m/s.

   Once the terminal velocity is calculated it may be combined with the drop size and number of drops to determine the total sound power level radiated from drops in the range 5-5.1mm. This process may be repeated for all other intervals and the results summed to arrive at the total radiated sound power level for the estimated natural rain.

## APPENDIX C

## TESTED ROOFING MATERIALS
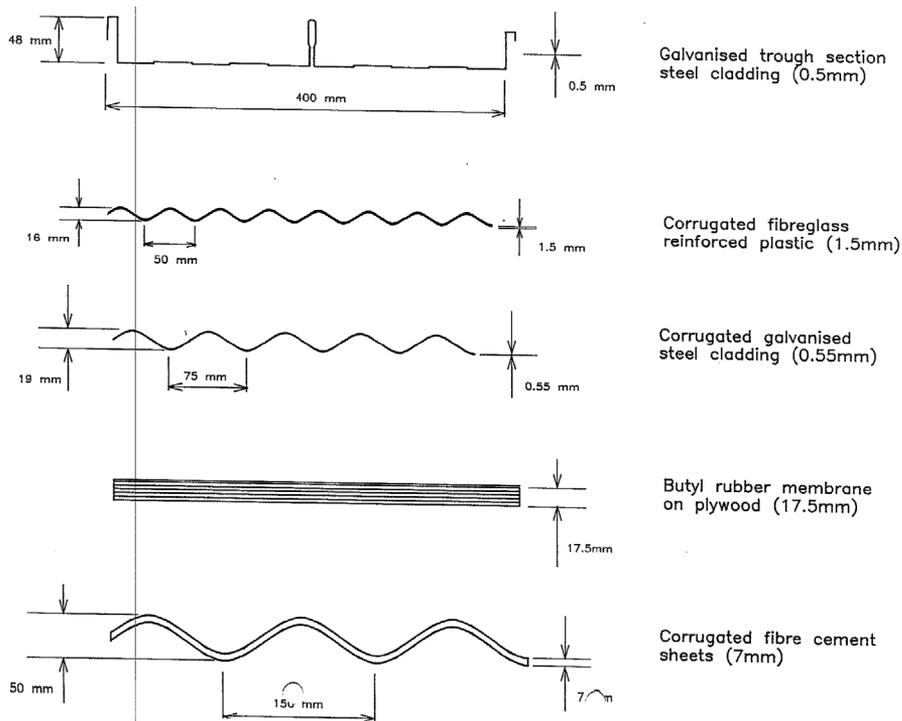


Figure 13.    Tested Roofing materials